Performance test and analysis of a high-capacity Stirling type pulse tube cryocooler with orthogonal room temperature displacers

Xiaotao Wang[1*], Shuai Chen[2*], Shengli Huang[2], Wei Dai[1], and Haibing Li[2]

[1] Key Laboratory of Cryogenic Science and Technology, Technical Institute of Physics and Chemistry, CAS. Beijing, China
[2] Lihan Cryogenics Co., Ltd. Shenzhen, China

[*]E-mail: xtwang@mail.ipc.ac.cn and shuai_chen@lihan.com

Abstract. Stirling-type pulse tube cryocoolers are known for their compact design, reliability, and long operational life, but traditional systems are primarily limited to small-scale cooling applications. To meet the growing demand for high cooling capacity in fields such as superconducting power transmission, small-scale gas liquefaction, and BOG (Boil-Off Gas) management, this paper presents a single-stage Stirling-type pulse tube cryocooler with orthogonal room temperature displacers. This design enhances the reliability of the displacer, as it operates at room temperature, thus improving reliability, and optimizes acoustic field distribution, leading to significant performance improvements over traditional pulse tube cryocoolers. By combining theoretical analysis with experimental validation, we examined the effects of key parameters, including pressure ratio, frequency, and displacer stiffness, on cooling capacity across cold head operating temperatures from 40 K to 100 K, considering working at different ambient temperatures. Experimental results show that the optimized cryocooler achieves a minimum temperature of 38.5 K and a cooling capacity of 325 W at 77 K, with an input power of 4.5 kW, demonstrating a relative Carnot efficiency of approximately 21.7%. The cryocooler has a total weight of 82 kg, making it suitable for applications where weight is a crucial factor.

1. Introduction

Regenerative cryocoolers, such as Gifford-McMahon (GM) and Stirling type, are widely used in various cryogenic applications, including gas liquefaction, superconducting magnets, infrared sensors, and biological storage[1], [2]. For applications requiring cooling capacities of several hundred watts at liquid nitrogen temperatures (~77 K), current commercial solutions typically include oil-lubricated rotary Stirling cryocoolers[3] or single-stage GM cryocoolers[4].

Oil-free Stirling-type cryocoolers driven by linear compressors eliminate lubricant contamination, enabling longer lifetimes and reduced maintenance. These cryocoolers have become attractive for sensitive applications like infrared detectors, superconducting electronics, and biological cryopreservation, but they typically operate at relatively low cooling powers. Most commercially available oil-free Stirling-type cryocoolers are limited to cooling powers below 100 W at 77 K[5], and there are few commercial options that extend these advantages to the several-hundred-watt range needed by mobile cryogenic systems and compact superconducting devices.

To meet the growing demand for high-capacity, oil-free Stirling-type cryocoolers, this study develops and evaluates a high-capacity, single-stage Stirling-type pulse tube cryocooler driven by an oil-free linear compressor. To combine the benefits of the pulse tube cryocooler's cold-end without moving parts and the effective phase control and expansion work recovery enabled by displacers, we apply a room-temperature displacer technology previously demonstrated in small-capacity systems[6]. Extending this approach to higher capacities requires careful optimization of design parameters and mechanical layout to achieve high performance, ease of manufacturing, and sustained efficiency as cooling power increases.

This paper first presents a theoretical analysis comparing different phase-shifting methods, then details the numerical modeling and mechanical design, and finally discusses comprehensive experimental test results. The results demonstrate the effectiveness of the OrthoCool™ configuration for efficient, reliable, and low-vibration, high-capacity cryogenic cooling.

2. Theoretical Analysis and Modelling

Figure 1 compares three types of linear-compressor-driven regenerative cryocoolers: the Stirling cryocooler, the inertance-type pulse tube cryocooler, and the room-temperature displacer cryocooler proposed in this work.

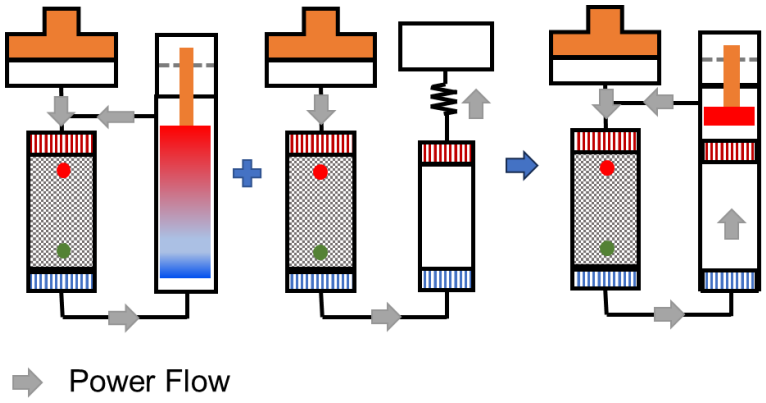

Figure 1. Regenerative cryocoolers: Stirling, pulse tube, and proposed ambient displacer configurations

The Stirling cryocooler (left) uses a mechanical displacer at the cold end to control the phase between pressure and flow. This design provides good efficiency and stable flow, but the cold-end displacer is difficult to manufacture and assemble, especially because of its long structure and the challenges of supporting it at low temperatures.

The pulse tube cryocooler (middle) removes the displacer with void tube and uses an inertance tube and gas reservoir to achieve phase shift. It has no moving parts at the cold end, making the system simpler and more reliable. However, the inertance tube consumes acoustic power and offers less efficient phase shift, resulting in lower overall efficiency.

To combine the advantages of both systems, we propose a new design that uses a room-temperature displacer. This approach keeps the cold end simple like a pulse tube, while enabling precise phase control similar to the Stirling cryocooler. It improves efficiency, simplifies manufacturing, and helps maintain a compact structure.

For phase control with a room-temperature displacer, two main configurations are possible: rod-less and rod-type designs (see Figure 2). The choice between these two directly impacts phase-shifting effectiveness, mechanical complexity, and system performance.

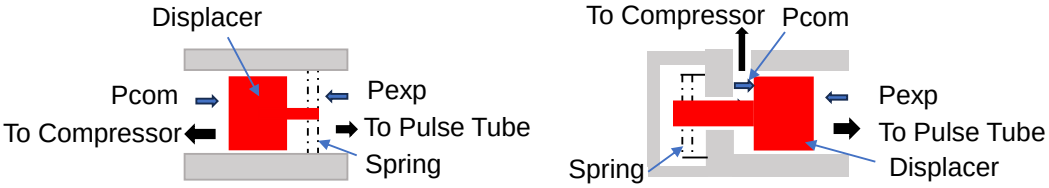

Figure 2. Schematic comparison of rod-less (left) and rod-type (right) ambient displacer.

In the rod-less configuration, the displacer is directly connected to a suspension spring. We have previously validated this structure in small-capacity cryocoolers, achieving up to 24% relative Carnot efficiency at liquid nitrogen temperatures[6]. The complex amplitude of the displacer velocity in response to the pressure difference between the expansion and compression sides, can be written as:

$$\hat{u}_d = \frac{(\hat{p}_{\exp} - \hat{p}_{\mathrm{com}})A_d}{i\omega m - ik/\omega + R_m} \tag{1}$$

Where $\hat{u}_d$ is Complex amplitude of the displacer velocity, $\hat{p}_{\exp}$ and $\hat{p}_{\mathrm{com}}$ are the complex pressure amplitudes on the pulse tube and compression sides, A_d is displacer area, m is total moving mass, k is spring stiffness and R_m is mechanical damping coefficient.

Due to pressure drop across the regenerator, the pressure amplitude of the pulse-tube-side is lower than on the compression side. As a result, the net force on the displacer is opposite to the direction of the acoustic power flow. This means that, to achieve the required phase shift between pressure and velocity, a large spring stiffness is needed, complicating mechanical tuning and increasing sensitivity to assembly tolerances.

In the rod-type configuration, the displacer piston is connected via a rod to a relatively large enclosed chamber on the compression side, where the internal pressure oscillation amplitude is much smaller than that in the expansion space, The complex amplitude of the displacer velocity can be written as:

$$\hat{u}_d = \frac{\hat{p}_{\exp}A_d - \hat{p}_{\mathrm{com}}(A_d - A_{rod})}{i\omega m - ik/\omega + R_m} \tag{2}$$

Where, A_{rod} is effective area of the rod.

In this configuration, the presence of the rod reduces the force acting on the displacer from the compression chamber, so the net force is mainly determined by the expansion side and thus aligns with the direction of acoustic power flow. This enables phase control with much lower spring stiffness, as the spring is mainly responsible for balancing the moving mass and tuning the resonance frequency close to the operating frequency. Although the rod and chamber add some structural complexity, they also provide space for implementing gas-bearing supports, which can improve stability and reduce friction. The additional sealing required is generally manageable if properly designed.

To further compare the two types of displacers, numerical simulations were performed using the Sage software platform [7]. Key component parameters were optimized and are summarized in Table 1.

Table 1. Detailed geometry and operating parameters of the cryocooler

Components	Details
Regenerator	Diameter 100 mm, length 60 mm, filled with 300# SS mesh
Pulse tube	Diameter 100 mm, length 100 mm
Piston swept volume	220 cm^3
Frequency	70 Hz
Displacer	Mass 280 g, Diameter 80 mm

Figure 3 shows the variation of cooling power and relative Carnot efficiency with flexure stiffness. The rod-less configuration gives higher simulated cooling power and efficiency, but requires a much larger spring stiffness—up to 150 kN/m. Under these conditions, the pressure oscillation at the warm end of the pulse tube leads the volume flow rate by 78.2°, resulting in a 60.5° phase lead at the cold end of the regenerator, while the regenerator hot end lags by 38.1°. The corresponding pressure drop across the regenerator is 38.4 kPa, yielding a cooling capacity of 415.5 W at 77 K with an input PV power of 3.23 kW.

In comparison, with a rod-type configuration using a 24 mm diameter rod, the system reaches its peak efficiency at a flexure stiffness of about 69 kN/m. In this case, the pressure oscillation at the warm end of the pulse tube leads the volume flow rate by 79.1°, giving a 62.9° phase lead at the regenerator cold end, while the regenerator hot end lags by 35.6°. The pressure drop across the regenerator is reduced to 33.5 kPa, producing a cooling capacity of 357 W at 77 K with an input PV power of 3.06 kW.

This poses challenges for mechanical implementation and stability. In practice, the rod-type displacer offers easier mechanical properties and still achieves competitive efficiency.

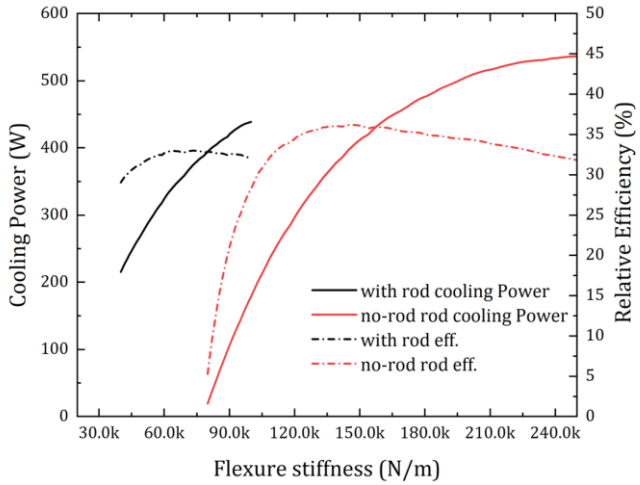

Figure 3. Performance comparison of rod and rod-less displacers versus flexure stiffness.

3. Cryocooler Orthogonal Design and Experimental Setup

3.1 Orthogonal Structural Innovation: OrthoCool™

Building upon the theoretical analysis and phase-shifting strategy described above, we developed a practical cryocooler system featuring a distinctive orthogonal mechanical layout. A key

innovation is the implementation of a distinctive orthogonal mechanical layout, referred to as OrthoCool™, in which the major components are distributed along three perpendicular axes: dual-opposed linear compressors along the X-axis, room-temperature displacers along the Y-axis, and the cold finger (comprising the regenerator and pulse tube) along the Z-axis.

The displacers are independently driven to precisely control the acoustic phase shift between pressure and flow—an essential factor in achieving high thermodynamic efficiency. The vertical orientation of the cold finger minimizes gravitational influence and simplifies mechanical support.

Beyond thermal and dynamic advantages, this configuration also reduces the stiffness requirements of the flexure springs in the displacer suspension, enabling more compliant design and lowering the risk of structural resonance. The mechanical decoupling between the cold finger and compressor, combined with the symmetric displacer arrangement, significantly suppresses vibration transmission to the cold-end. Additionally, the modular and orthogonal structure simplifies manufacturing and assembly, ultimately reducing system cost and improving maintainability.

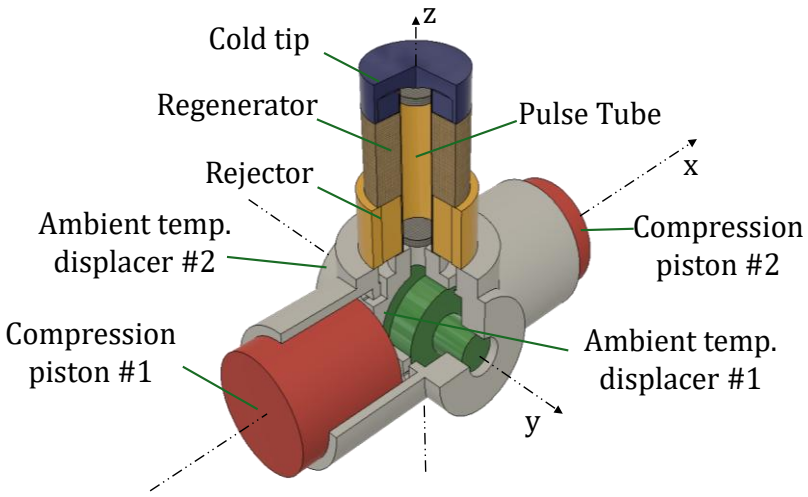

Figure 4. Orthogonal structural layout of the cryocooler

3.2 Experimental Setup

The complete cryocooler assembly measures approximately 580 mm × 470 mm × 310 mm (L × H × W), with a total system mass of 82 kg, making it suitable for benchtop operation. The system is powered by a custom-designed variable-frequency controller capable of delivering up to 6 kW, with a power conversion efficiency exceeding 90%, ensuring precise acoustic power input and efficient operation.

Temperature measurements were conducted using calibrated PT100 sensors with an accuracy of ±0.1 K, installed at key locations such as the cold head and aftercooler. Dynamic motion of the pistons and displacers was monitored using linear variable differential transformers (LVDTs), while compressor input power was measured by the power controller.

A LabVIEW-based data acquisition system was employed to record all sensor signals synchronously. The working fluid was helium, charged to a mean pressure of 3.5 MPa. During testing, the compressor operated at frequencies ranging from 60 to 70 Hz, with piston stroke controlled to remain below 11 mm. Cooling water was maintained at a stable temperature via a closed-loop chiller.

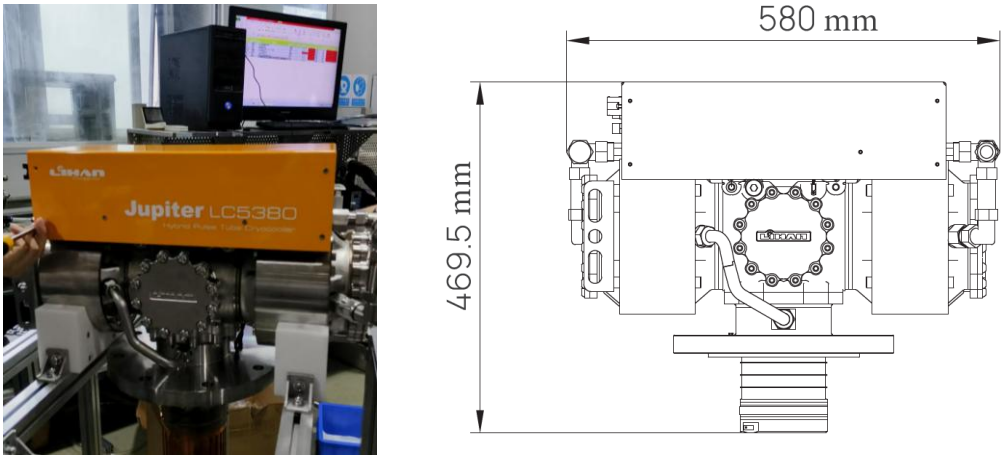

Figure 5. Compact structural layout of the developed single-stage, linear compressor-driven pulse tube cryocooler: experimental setup (left) and dimensional drawing (right).

Both no-load and load conditions were tested. In no-load tests, the minimum cold-head temperature and temperature stability were recorded. In load tests, electrical heaters were mounted on the cold-end heat exchanger to apply controlled thermal input for performance evaluation.

4. Experimental Results and Discussion

4.1. No-Load Temperature and Stability

Figure 6 shows the typical cool-down behavior of the cold head under no-load condition. The cryocooler was operated at a mean pressure of 3.5 MPa, a frequency of approximately 65 Hz, a cooling water temperature of 20 °C, and an input electrical power around 2.8 kW. The cool-down rate is primarily determined by the heat capacity of the object being cooled, and the cold-end heat exchanger, made of copper, has a mass of 4.08 kg. Under no-load conditions and without any other attached thermal mass, the cold-head temperature decreased continuously from ambient to below 40 K within approximately 18 minutes, reaching a lowest no-load temperature of 38.5 K. Within a few minutes, the temperature stabilized at this level, with fluctuations limited to approximately ±0.01 K RMS.

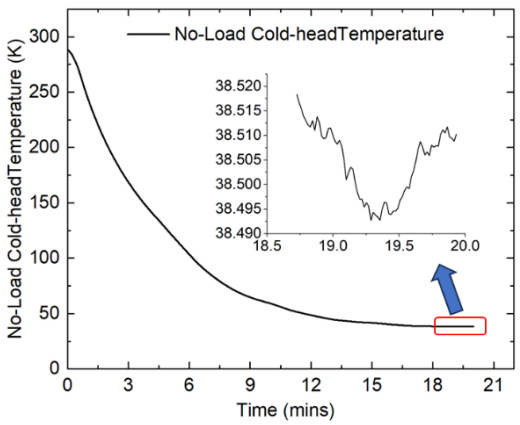

Figure 6. Cool-down curve of the no-load cold head and temperature stability at steady state

4.2. Cooling Capacity and Performance Analysis

The cooling capacity of the cryocooler was systematically measured over a broad range of operating conditions. Throughout the entire set of tests at different cold-head temperatures, the operating conditions for both the experiment and simulation were kept consistent, including charge pressure, drive frequency, and piston stroke. The measured and simulated cooling powers under two ambient rejection conditions (20 °C and 35 °C) are shown in Figure 7 As shown, a cooling performance improvement of approximately 6% was observed when the ambient temperature was reduced from 35 °C to 20 °C.

At higher cold-head temperatures, the simulation results agreed well with the experimental data. However, as the temperature decreased, the simulations tended to overpredict the cooling capacity. At an input power of 4.2 kW, the cryocooler provided 325 W of cooling at 77 K, corresponding to a relative Carnot efficiency of 21.7%. As the cold-head temperature increased, the efficiency rose to a maximum of 24%.

At lower cold-head temperatures and higher cooling capacities, the difference between the simulation and experimental results became larger. This was likely caused by greater cooling losses due to higher gas flow rates or larger temperature differences. These results suggest that the current simulation model does not fully reflect the effects of complex gas flow inside the cold head, indicating that improvements are needed in both the model and the experimental setup to achieve better accuracy.

Figure 8 presents the measured and simulated compressor input power and relative Carnot efficiency across a range of cold-head temperatures. Both the measured and simulated input power decreased gradually as the cold-head temperature increased. This trend is attributed to the higher acoustic impedance of the cold head at lower temperatures, which allows the compressor to deliver more acoustic power under the same piston swept volume. The simulated input power was consistently lower than the measured values throughout the temperature range.

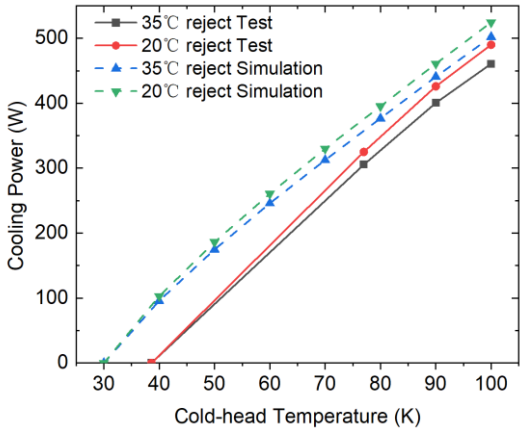

Figure 7. Measured and simulated cooling power at different cold-head temperatures under two ambient rejection conditions.

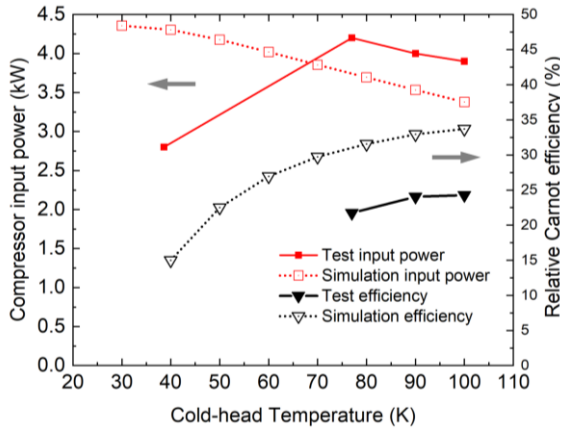

Figure 8. Measured and simulated compressor input power and relative Carnot efficiency versus cold-head temperature.

The measured relative Carnot efficiency ranged from 21% to 24%, while the simulation predicted higher values, reaching up to 34%. The overestimation of both cooling capacity and efficiency suggests that the current numerical model does not fully account for key loss mechanisms, including internal flow resistance, regenerator friction, and complex flow behavior

within the pulse tube. Improving the accuracy of input power estimation and efficiency prediction will be essential for refining the model and optimizing future cryocooler designs.

5. Conclusions

A high-capacity, single-stage, oil-free pulse tube cryocooler driven by a linear compressor was developed and tested. Based on theoretical analysis and structural optimization, an orthogonally arranged room-temperature displacer configuration was adopted to improve efficiency and simplify fabrication. A prototype was built and successfully tested.

The system has a compact, modular design with a total mass of 82 kg, making it suitable for applications with strict volume, weight, and efficiency requirements. It achieved a cooling capacity of 325–380 W at 77 K, a minimum no-load temperature of 38.5 K, and a relative Carnot efficiency of up to 21.7%.

The orthogonal structure was effective for phase control, vibration suppression, and system integration. Experimental results showed good agreement with simulation trends, though differences in absolute values suggest that current models need refinement to better reflect internal flow and acoustic losses.

Future work will focus on increasing cooling power, improving efficiency, and adapting the system for practical use. More accurate modeling and a deeper understanding of flow behavior will help guide future design improvements.

Acknowledgments

This work is financially supported by the National Key Research and Development Program of China (No. 2022YFF0712600) and the National Natural Science Foundation of China (No. 51976231).

References

[1] R. Radebaugh, “Cryocoolers: the state of the art and recent developments,” *J. Phys.: Condens. Matter*, vol. 21, no. 16, p. 164219, Apr. 2009, doi: 10.1088/0953-8984/21/16/164219.
[2] D. A. Cardwell, D. C. Larbalestier, and I. B. Aleksander, *Handbook of Superconductivity: Fundamentals and Materials, Volume One*, 2nd ed. Boca Raton: CRC Press, 2022. doi: 10.1201/9780429179181.
[3] D. Sun, Y. Xu, and Q. Shen, “An efficient high cooling capacity Stirling cryocooler and its application for capturing boil-off methane from liquefied natural gas,” *International Journal of Refrigeration*, vol. 165, pp. 425–433, Sep. 2024, doi: 10.1016/j.ijrefrig.2024.06.013.
[4] S. K. Gandla, M. Xu, J. Koch, S. Dunn, and R. C. Longworth, “Development of High-Capacity Single-Stage GM Cryocooler,” *Cryocoolers 22, edited by R.G. Ross, Jr., J.R. Raab and S.D. Miller, International Cryocooler Conference, Inc., Boulder, CO, 2022, pp.249-254*
[5] H. Li *et al.*, “Advances in Pulse Tube Cooler with Dual-opposed Ambient Temperature Displacers,” *IOP Conf. Ser.: Mater. Sci. Eng.*, vol. 1301, no. 1, p. 012144, May 2024, doi: 10.1088/1757-899X/1301/1/012144.
[6] X. Wang *et al.*, “A high efficiency hybrid stirling-pulse tube cryocooler,” *AIP Advances*, vol. 5, no. 3, p. 037127, Mar. 2015, doi: 10.1063/1.4915900.
[7] D. Gedeon, “Sage: Object-Oriented Software for Cryocooler Design,” in *Cryocoolers 8*, R. G. Ross, Ed., Boston, MA: Springer US, 1995, pp. 281–292. doi: 10.1007/978-1-4757-9888-3_28.